Development and Assessment of Resource Management Solutions for Throughput Enhancement in a RIS-aided Mobile Network

Agarwal, Sakshi; Das, Kallol; Litjens, Remco

DOI
10.1109/EuCNC/6GSummit60053.2024.10597054

Publication date
2024

Document Version
Final published version

Published in
2024 Joint European Conference on Networks and Communications and 6G Summit, EuCNC/6G Summit 2024

2024 EuCNC & 6G Summit - RAS 1570991174
2024 Joint European Conference on Networks and Communications & 6G Summit (EuCNC/6G Summit): Radio Access and Softwarisation (RAS)

Development and Assessment of Resource Management Solutions for Throughput Enhancement in a RIS-aided Mobile Network

Sakshi Agarwal*, Kallol Das*, Remco Litjens*†
* Department of Networks, TNO, The Hague, The Netherlands
† Faculty of EEMCS, Delft University of Technology, Delft, The Netherlands
Email: *{sakshi.agarwal, kallol.das, remco.litjens}@tno.nl

***Abstract*—Reconfigurable Intelligent Surfaces (RIS) stand out among the key technologies driving 6G mobile network development. In this paper, we develop and assess radio resource management solutions aimed to exploit the potential of RIS deployments for coverage and throughput enhancement for indoor users in 6G mobile networks. We introduce two heuristic algorithms that jointly control the cell-RIS-user association, user scheduling, transmit beamforming and the RIS's reflective configuration, and compare these algorithms against a RIS-free benchmark. Simulation results are presented to *(i)* demonstrate the promising potential of RIS deployments in multi-cell/multi-user scenarios; *(ii)* reveal the inherent trade-off between coverage and throughput enhancement; and *(iii)* show the performance impact of distinct RIS deployment locations. Our study provides valuable insights for efficiently leveraging RIS in evolving mobile network architectures.**

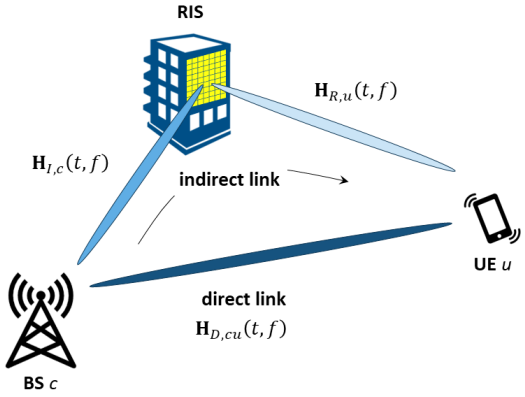

Fig. 1. Visualisation of the direct cell-user and indirect cell-RIS-user links.

I. Introduction

The deployment of 5G technology has significantly transformed the wireless communication landscape, supporting enhanced mobile broadband, massive machine-type communications and ultra-reliable low-latency services. The envisioned 6G technology is targeted to support internet speeds up to terabits per second, ubiquitous connectivity, AI-driven network management, and support for advanced applications such as immersive eXtended Reality (XR), and sophisticated Internet of Things (IoT) systems. Achieving this ambitious vision requires the incorporation of several potential enablers, including network ultra-densification, the use of sub-THz spectrum, integrated sensing and communications, and the use of Reconfigurable Intelligent Surfaces (RISs) [1].

RISs are programmable arrays composed of sub-wavelength sized meta-surface elements with a controllable impedance [1], enabling the dynamic adaptation of the element-specific phase shifts and, consequently, the reflective properties of the RIS (passive beamforming). This adds a degree of operational flexibility allowing the effective control of the propagation environment, which can be exploited to enhance network performance across diverse scenarios. For example, RISs can be used to extend coverage to challenging areas and enhance multipath propagation environments, as illustrated in Figure 1. Unlocking the full potential of RIS technology involves addressing key challenges related to the design and deployment of large-scale RIS systems, accurate acquisition of Channel State Information (CSI) and effective control of RIS in dynamic propagation environments.

A comprehensive literature review reveals a number of noteworthy efforts in the control of RISs in a mobile network. Considering a single-cell scenario, [2] introduces a semi-definite relaxation and alternating optimization algorithm for joint optimization of base station precoding (active beamforming) and RIS configuration. Alternatively, [3] employs fixed-point iteration and manifold optimization techniques to enhance signal strengths. Furthermore, RIS optimization utilising machine learning-based methodologies such as deep reinforcement learning [4] and deep neural networks [5] are developed to tackle the inherent computational complexity associated with the aforementioned joint optimization problem. Generally focusing on single-cell scenarios, studies often overlook resource management challenges such as RIS-aware scheduling and cell-RIS-UE (User Equipment) association, which are of particular relevance in multi-cell scenarios. Although some studies, including those utilizing graph neural networks [6] and deep reinforcement learning [7], attempt to tackle these challenges, the addressed scenarios often lack key realistic aspects related to e.g. the dynamics of propagation or traffic aspects or the possibility of multi-user MIMO transmission. This leaves a notable research gap in RIS deployment strategies and associated resource management challenges.

To the best of our knowledge, this work presents the first attempt to develop and assess radio resource management solutions exploiting RIS deployments towards coverage and throughput enhancement in multi-cell/multi-user scenarios. We herein analyse distinct algorithms addressing cell- and RIS-UE association, scheduling and the joint optimization of beamforming (cell) and reflection (RIS) parameters. We assess

the attainable performance of the proposed algorithms against a RIS-free benchmark solution considering distinct scenarios in terms of network size, RIS deployment locations and the presence of temporary blockers with varying strengths.

The remainder of the paper is organized as follows. Section II describes our key modelling assumptions. Section III presents the problem statement and the developed control solutions. Simulation-based performance results are discussed in Section IV, with key conclusions summarized in Section V.

II. Modeling

In this section, we describe the key modelling aspects relevant for the assessment study, including network aspects, a RIS model and a characterisation of the propagation environment.

A. Network aspects

We consider a network comprising N_C cells served by directional antennas which are deployed in a hexagonal layout with an inter-site distance of 500m, representing a dense urban deployment [8]. Figure 2 depicts the addressed single- ($N_C = 1$) and multi-cell ($N_C = 19$) scenarios. Each cell is assigned a TDD (Time Division Duplex) carrier in the 3.5 GHz band with a carrier bandwidth of $BW = 20$ MHz and the TDD frame configured with a 4:1 down- versus uplink resource split. We assume use of a 30 kHz numerology, thus implying a TTI (Transmission Time Interval) duration of 0.5ms and the availability of N_{PRB} = 50 PRBs (Physical Resource Blocks). The total transmit power per cell is $P_T = 120$W. The BS (Base Station) height is fixed at $H_{BS} = 25$m.

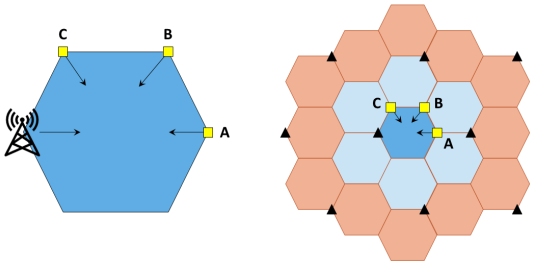

Fig. 2. Considered single- (left) and multi-cell (right) network layouts.

In the multi-cell scenario, the performance assessment concentrates only on the UEs served in the center (dark blue) cell, while a realistic interference environment is approximated by explicitly simulating UEs in the adjacent tier of (light blue) cells and assuming fixed-power transmissions in the outermost (red) cells. Each blue-colored cell is equipped with a 64T64R antenna array deployed with a 5° mechanical downtilt. The antenna array comprises 8 rows and 4 columns of two cross-polarized antenna elements (AEs) with half-wavelength ($\lambda/2$) inter-AE spacing, yielding a total of $N_{TX} = 64$ AEs. The individual AEs are modelled as specified in Table 7.3-1 of [8] with a maximum gain of 8 dBi. As mentioned above, the red-colored cells in the outer tier do not serve explicitly modelled UEs, yet are assumed to continuously transmit at maximum power P_T with an effective antenna diagram taken from [9], also including a 5° mechanical downtilt.

The traffic is characterised by the presence of N_U UEs, which are uniformly distributed over the blue cells and engaged in persistent downlink data transfers. The UEs have a height of $H_{UE} = 1.5$m, are assumed to be locally mobile at pedestrian speed and are located indoors. Each user device features two pairs of cross-polarised AEs placed in opposite corners (hence $N_{RX} = 4$ AEs) with a per-AE antenna gain of 0 dBi.

B. RIS model

A single RIS is assumed to be deployed at candidate position A, B or C depicted in Figure 2, mounted to a building at a height of $H_{RIS} = 20$m and with the indicated orientations. The modelled RIS comprises $M = 40 \times 40 = 1600$ meta-surface elements of size $\lambda/2 \times \lambda/2$, arranged in a square array with half-wavelength inter-element spacing.

Each RIS element reflects the signal with a controllable phase shift and no amplitude attenuation. We denote with $\mathbf{\Phi}$ the diagonal RIS configuration matrix containing the polar-form representations $e^{j\theta_m}$ of the element-specific phase shifts θ_m, for $m = 0, \cdots, M-1$. Although in practice the phase shifts may be restricted to a limited set of discrete options, we assume an infinite phase granularity and model the θ_m as continuous complex variables, noting that even a phase quantisation into only three bits already suffices to prevent any significant performance loss [10]. The default RIS configuration $\mathbf{\Phi}_d = \boldsymbol{I_M}$, i.e. the identity matrix of size M, is applied used when the RIS is not optimised to reflect signals in any specific direction. With this setting all elements are configured with a common phase shift, the RIS acts as a mirror and consequently reflects with maximum gain in the direction where the reflected angle is equal to the incident angle [11].

C. Propagation environment

In the considered connectivity setting, a distinction is made between three types of radio links, viz. the direct link (labelled 'D') between a given cell c and UE u, and the indirect cell-RIS-UE link comprising a link (labelled 'I': incident signal) between cell c and the RIS, and a link (labelled 'R': reflected signal) between the RIS and UE u, as visualised in Figure 1.

For a given PRB f and TTI t, the channel response matrix associated with these links is denoted by $\mathbf{H}_{D,cu}(t,f) \in C^{N_{TX} \times N_{RX}}$, $\mathbf{H}_{I,c}(t,f) \in C^{N_{TX} \times M}$ and $\mathbf{H}_{R,u}(t,f) \in C^{M \times N_{RX}}$, respectively. Considering the combination of the direct and indirect links, a cascaded channel model is used to describe the effective cell-RIS-UE channel, given by

$$\mathbf{H}_{cu}(t,f) = \mathbf{H}_{D,cu}(t,f) + \mathbf{H}_{I,c}(t,f)\mathbf{\Phi}(t)\mathbf{H}_{R,u}(t,f)$$

with $\mathbf{\Phi}(t)$ the RIS configuration matrix applied at TTI t [3]. When deriving the assumed wideband precoders (at the BS) and RIS configuration matrices, we make use of the appropriately wideband-averaged channel response matrices, denoted $\bar{\mathbf{H}}_{D,cu}(t)$, $\bar{\mathbf{H}}_{I,c}(t)$, $\bar{\mathbf{H}}_{R,u}(t)$ and $\bar{\mathbf{H}}_{cu}(t)$, respectively.

The urban propagation environment is characterised by a modelling of *(i)* the average channel characteristics, including the effects of antenna gain, path loss, shadowing, blocker loss, body loss, building penetration loss, a so-called 'RIS orientation loss' and a 70 dB minimum coupling loss; and *(ii)* small-scale fading. We herein assume that the RIS is carefully deployed to ensure an unobstructed line of sight (LOS) path

between the associated center cell and the RIS, thus avoiding any shadowing or blocking effects on the cell-RIS link.

A log-distance *path loss* model is used for each link, using the Friis model [12] for the cell-RIS link and the 3GPP UMa NLOS (urban macro; non-LOS) model [8] for the cell-UE and RIS-UE links. Only for the cell-UE and RIS-UE links, *shadowing* is applied and modelled as a zero-mean Gaussian random variable with a standard deviation of 6 dB [8]. The spatial and inter-site shadowing correlation are modelled by generating a set of cell- and RIS-specific shadowing maps, created using the methodology of [13] and considering a decorrelation distance of 50m and an inter-site correlation of 0.5 [13]. In addition to shadowing, the *blocking loss* models the randomised presence and attenuation effects of specific blocking objects, e.g. a large truck, on the cell-UE and/or the RIS-UE links. The blocker loss is modelled by the probability of occurrence $P_{BL} = 0.2$ and, in case of occurrence, the blocker loss BL, which will be varied. Further, we assume a *body loss* of 6 dB [14] and a *building penetration loss* as modelled in Table 7.4.3-3 of [8]. Since the RIS is assumed to be deployed on a building facade, there is no indirect path when a cell or UE is located behind the building, which is modelled by a *RIS orientation loss* of ∞ dB.

For the unobstructed cell-RIS link, *small-scale fading* depends purely on the relative distance between the transmit antenna and the RIS elements, given by $\mathbf{H}_{I,c}^{ss}[i,j] = e^{j2\pi d_{ij}/\lambda}$ for cell c, its transmit antenna element $i = 0, \cdots, N_{TX} - 1$, RIS element $j = 0, \cdots, M-1$, with d_{ij} the distance between these two elements and λ the carrier wavelength. For the cell-UE and RIS-UE links, we characterise small-scale fading based on the UMa model as specified in [8] with implementations provided by [15]. Herein we assume local user mobility at a pedestrian speed of 0.8 m/s.

III. Problem statement and heuristic solutions

This section describes the addressed research problem and details the proposed control solutions. Key objective of this research is to assess the throughput enhancement potential of the deployment and optimised exploitation of a RIS in a mobile network, jointly addressing the challenges of cell-UE association, UE scheduling, RIS-UE association (assignment of the RIS to a scheduled UE) massive MIMO beamforming and RIS configuration. To this end, two distinct control algorithms will be proposed and compared against a benchmark solution.

Before detailing the benchmark and proposed control solutions, we note that a static cell-UE association is considered. A UE selects its serving cell based on the average received SSB (Synchronization Signal Block) Reference Signal Received Power (SSB-RSRP), provided that signal power exceeds the coverage threshold of -120 dBm. Otherwise the UE is considered out of coverage. When performing the coverage check and the cell-UE association in the benchmark algorithm (Algorithm 0) and in Algorithm 1, the RIS is assumed to tuned to its default configuration $\mathbf{\Phi}_d$, while in Algorithm 2 we assume an idealistic, UE-specific coverage-optimised RIS configuration maximising the coverage.

Benchmark *Algorithm 0* assumes the RIS is deployed and is statically configured to its default configuration $\mathbf{\Phi}_d$. The reason to still include the RIS's presence in the benchmark case and effectively assume the explicit presence of a reflecting building at the given location, is to allow a fair comparison of algorithms by considering the same basic propagation environment. The assumed scheduler integrates an adaptation of the semi-orthogonal user scheduling (SUS) algorithm [16] with a proportional fairness (PF)-based UE ranking [17]. Addressing an upcoming TTI t and UE u, the PF ratio is given by $PF_u(t) = \tilde{R}_u(t)/\hat{R}_u(t-1)$, with $\hat{R}_u(t-1)$ the average data rate experienced so far and $\tilde{R}_u(t)$ the UE's expected instantaneous data rate, assuming single-user scheduling, Maximum Ratio Transmission (MRT)-optimised beamforming, a consequent estimation of the signal-to-interference-plus-noise ratio (SINR) $\tilde{\Gamma}_u(t)$ and applying the idealistic Shannon-Hartley formula for SINR to bit rate mapping. Going through the PF-ordered list, the adapted SUS scheme successively schedules UEs, provided that the estimated channels towards each newly selected UE satisfy an orthogonality criterion (configured by a threshold $\gamma = 0.5$; see [16]) w.r.t. those of already selected UEs. Given the resulting set of scheduled UEs, the eventual precoding matrix is derived using Zero Forcing (ZF), the SINRs $\Gamma_u(t)$ are determined, now including power sharing by the scheduled UEs, the SINRs are mapped to the applied data rates and, lastly, the average rate for each UE is updated using $\hat{R}_u(t) = \alpha\hat{R}_u(t-1) + (1-\alpha)R_u(t)$, with $\alpha = 0.1$ the applied exponential smoothing coefficient.

Algorithm 0 (Benchmark algorithm)

for all UE u **do**
  Assign UE u to the cell with the highest SSB-RSRP
end for
for all TTI t **do**
  for all UE u **do**
    Derive MRT precoder
    Determine SINR $\tilde{\Gamma}_u(t)$
    Derive data rate $\tilde{R}_u(t) = BW\log_2(1+\tilde{\Gamma}_u(t))$
    Calculate $PF_u(t) = \tilde{R}_u(t)/\hat{R}_u(t-1)$
  end for
  Aggregate the $PF_u(t)$ values in sorted vector $\mathbf{u}_{ordered}$
  Initiate SUS algorithm by scheduling UE $\mathbf{u}_{ordered}[0]$
  for i such that $0 < i \leq$ length$(\mathbf{u}_{ordered}) - 1$ **do**
    Co-schedule UE $\mathbf{u}_{ordered}[i]$ | channel orthogonality
  end for
  Derive ZF precoders for all scheduled UEs
  for all UE u **do**
    Determine SINR $\Gamma_u(t))$
    Derive data rate $R_u(t) = BW\log_2(1+\Gamma_u(t))$
    Update $\hat{R}_u(t) = \alpha\hat{R}_u(t-1) + (1-\alpha)R_u(t)$
  end for
end for

Newly proposed *Algorithm 1* jointly optimizes scheduling, RIS-UE association, beamforming and RIS configuration. As it is part of the scheduling decision for which UE the RIS configuration is optimised, we first derive for each UE separate PF values for the cases that the RIS is or is not optimised for that UE, denoted $PF_{u,RIS}(t)$ and $PF_u(t)$ (derived as under Algorithm 0), respectively. To determine the former, we derive the RIS configuration $\Phi_u(t)$ which optimises for UE u the effective cell-RIS-UE channel using the fixed-point optimization algorithm presented in [3]. Given the UE-optimised RIS configuration, the MRT precoder is determined

based on the updated channel. Aggregating all $PF_u(t)$ and $PF_{u,RIS}(t)$ ratios in a single ordered list, the adapted SUS scheme goes down the list and successively schedules UEs, while always appropriately verifying the channel orthogonality criterion. Key adjustment to the SUS procedure of Algorithm 0 here is that, once a UE is scheduled based on its $PF_{u,RIS}(t)$ value, this implies that the RIS is associated with that UE, and the remaining $PF_{u,RIS}(t)$ ratios are removed from the list, to ensure that the RIS is assigned to a single UE only.

Algorithm 1-2 (Proposed algorithms)

for all UE u **do**
  if Algorithm 1 **then**
    Conduct Step 2 of Algorithm 0
  else if Algorithm 2 **then**
    Conduct cell-UE association as in Algorithm 0 with an extra gain of M^2 on all links from the center cell
  end if
end for
for all TTI t **do**
  for all UE u **do**
    Calculate $PF_u(t)$ using Steps 6-9 of Algorithm 0
    Derive UE-optimised RIS configuration Φ_u
    Calculate $PF_{u,RIS}$ using Steps 6-9 of Algorithm 0 and assuming the RIS-optimised channel
  end for
  Aggregate the $PF_u(t)$ and $PF_{u,RIS}(t)$ values in sorted vector $\mathbf{u}_{ordered}$
  Initiate SUS algorithm by scheduling UE $\mathbf{u}_{ordered}[0]$
  for i such that $0 < i \leq \text{length}(\mathbf{u}_{ordered}) - 1$ **do**
    Co-schedule UE $\mathbf{u}_{ordered}[i]$ | channel orthogonality
    Remove remaining $PF_{u,RIS}$ from $\mathbf{u}_{ordered}$ once the RIS is assigned to a UE
  end for
  Conduct Steps 16-21 of Algorithm 0, assuming the RIS-affected channels in Step 16
end for

Both Algorithms 0 and 1 assume the RIS configuration is not optimised for the SSB reference signal and hence plays no active role in the cell-UE association and the coverage checks. In order to investigate the coverage-enhancing potential of RIS optimisation, we investigate *Algorithm 2*, which idealistically assumes that in the cell-UE association and coverage checks, the RIS configuration is optimised to perfectly reflect the SSB reference signal in the direction of the UE. To model this, an additional gain of M^2 is added to the average channel gain in the indirect link from the (RIS-associated) center cell to the UEs. As the results will demonstrate, this results in an enhanced coverage and an occasionally different cell-UE association. Apart from this difference, Algorithm 2 applies the same scheduling, RIS-UE association, beamforming and RIS configuration logic as Algorithm 1.

IV. Results

We have implemented the models of Section II and the algorithms of Section III into a system-level simulator, used to conduct an extensive performance assessment study. In this section we present the key results, referring to [18] for a more extensive set of numerical experiments. We first describe the key performance indicators (KPIs) and the considered scenarios, followed by a discussion of the obtained results.

As mentioned in Section II, the performance assessment concentrates on the UEs simulated in the (dark blue) center cell depicted in Figure 2. For these UEs, we evaluate both the *coverage probability*, defined as the fraction of simulated UEs that are covered by at least one of the cells; and the 10^{th} *user throughput percentile*, determined over all UEs in all simulated snapshots. Furthermore, we determine the *RIS network usage ratio* as the fraction of downlink TTIs in which the RIS configuration is actively optimised to enhance performance.

The addressed simulation scenarios cover a sensitivity analysis w.r.t. the presence and significance of the blocker loss BL (varied between 0 and 45 dB) and the RIS deployment location (see the candidate locations A, B, C indicated in Figure 2) and consider both single- and multi-cell scenarios, with results presented for the different performance metrics and scenarios in Figures 3 and 4, respectively. In either figure, Charts a, b and c assume RIS location A, while Chart d assumes a blocker loss of $BL = 30$ dB. The legend at the top indicate the colors used for the different algorithms, noting that in Chart d the bar charts depict the 10^{th} user throughput percentile and the dashed lines depict the coverage probability, following the primary and secondary axes, respectively.

In the upcoming subsections, we will consecutively discuss the simulation results for the single- and multi-cell scenarios.

A. Single-cell scenario

Consider Figure 3. Observe from Figure 3a that for all three algorithms the coverage probability decreases in the blocker loss, which is intuitively clear from the impact of the blocker loss on the SSB received power level, even if some UEs may find another covering cell as their serving cell. A more interesting observation is that Algorithm 2 substantially outperforms both benchmark Algorithm 0 and Algorithm 1, which is due to the fact that (only) Algorithm 2 exploits the RIS in enhancing the SSB coverage. This argument is strengthened by the fact that Algorithm 2 results in a higher RIS network usage than Algorithm 1, as seen in Figure 3c.

Figure 3b shows a non-monotonous dependency of the 10^{th} user throughput percentile w.r.t. the blocker loss. This reflects the conflicting effects of an increase in blocker loss. For the lower range of blocker loss values, the dominant effect we observe is that a higher blocker loss worsens the channel of a covered UE which has a blocker present on its direct and/or indirect link, and hence decreases the experienced throughput. However, for higher values of the blocker loss, the channel worsens more dramatically down to the level where it significantly affects coverage and, with fewer UEs actually served and sharing a common resource, an increasing effect on the user throughput performance. Observe that the fruitful RIS utilisation leads to higher throughputs under Algorithm 1 when compared to the benchmark case. Since Algorithm 2 (also) exploits the RIS for coverage enhancement, the higher number of served UEs implies a higher degree of competition for shared resources, and consequently a less significant throughput improvement.

Next we analyse the impact of RIS deployment location on coverage and throughput performance, see Figure 3d.

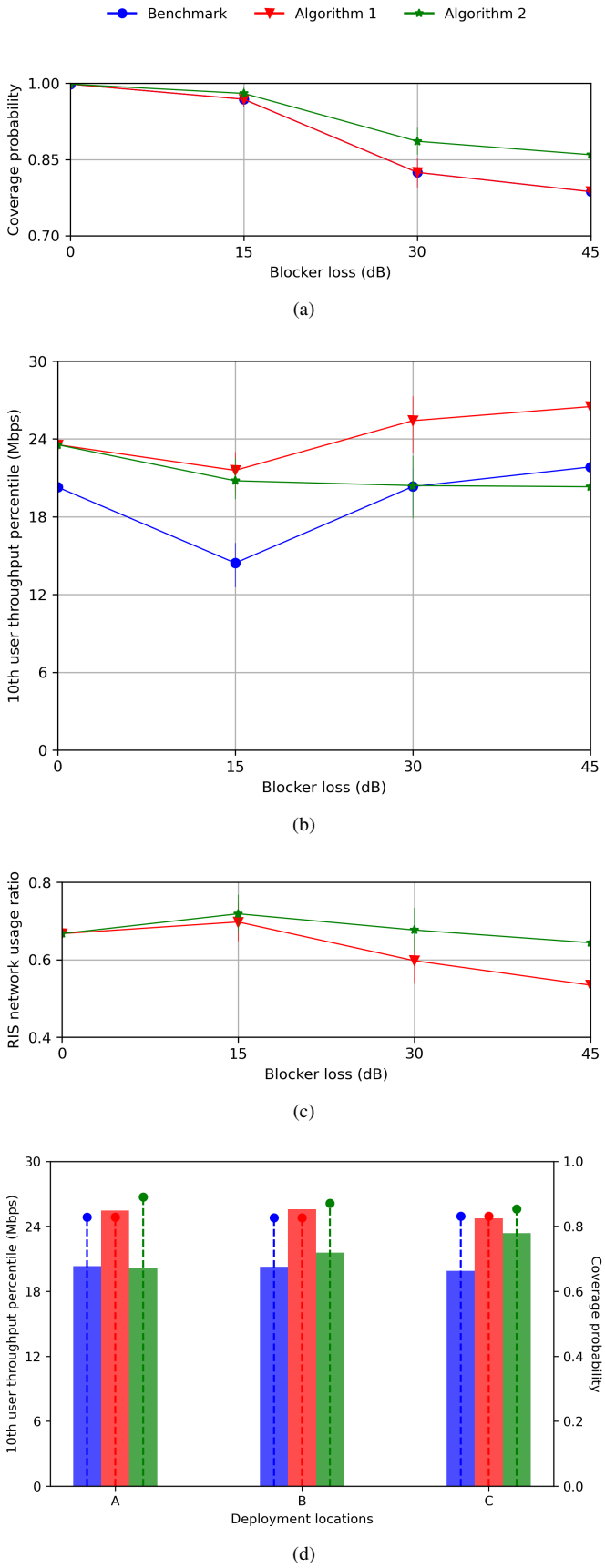

Fig. 3. Simulation results for the single-cell scenario.

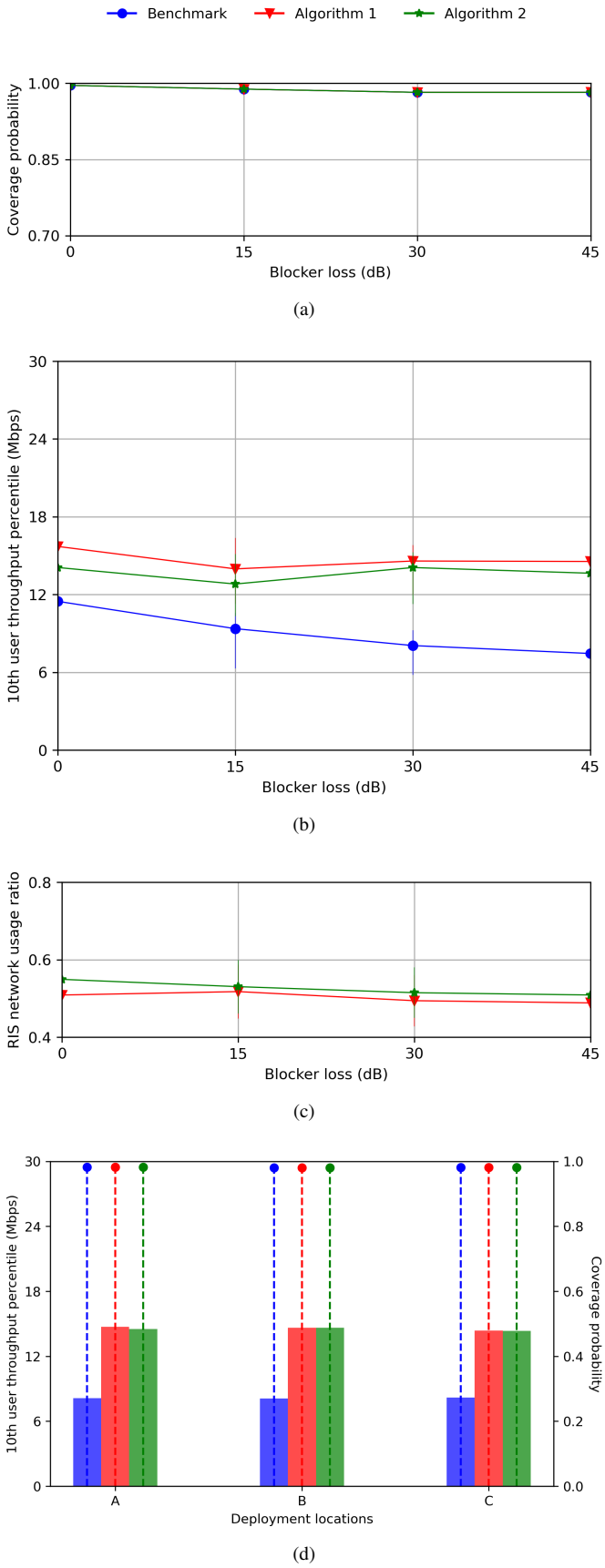

Fig. 4. Simulation results for the multi-cell scenario.

Obviously the RIS location does not affect the KPIs under the benchmark algorithm as it does not use the RIS. While both proposed algorithms improve user throughput, the specific RIS location minimally affects the gains. The RIS location impacts which UEs benefit and to what degree use of the RIS enhances their performance, with the bottom-line performance effect being rather similar for the distinct locations considered. For example, for a RIS deployed close to the cell site (location C), we observe that relatively few UEs experience a substantial throughput gain thanks to the improved indirect channel, while the direct channel of most UEs in the area is already so strong that peak bit rates are achieved or approached even without using the RIS, and hence for them the RIS offers little benefit. On the other hand, when a RIS is deployed near the cell edge (location A), many UEs in the area benefit from utilising the RIS, while the attained throughput gain on a per user level tends to be rather modest, due to the inherent weakness of the (long-distance) cell-RIS link. Another trade-off is visible under Algorithm 2 where the use of RIS results in an intuitively expected better coverage for RIS deployment at cell edge location A compared to location C, which consequently leads to a lower 10^{th} user throughput percentile for RIS location A.

B. Multi-cell scenario

Consider now Figure 4 for the multi-cell scenarios. We first observe from Figure 4a that across the range of blocker loss values, almost all UEs remain covered and the loss in coverage is very small. This is due to the fact that even if a blocker with a high loss is present on a given cell-UE link, in the considered dense urban network deployment scenario the UE may likely still be covered by another cell. Figure 4b shows a similar non-monotonous trend for the 10^{th} user throughput percentile as we had observed for the single-cell scenario, which had been explained to be due to the contradictory effects of an increasing blocker loss. Despite the intricate effects of the blocker loss, it is evident from the results that using the RIS by either Algorithm 1 or 2 substantially improves the user throughput performance compared to the benchmark.

Figure 4d again shows that the RIS deployment location does not have a large performance effect, following the same intuitive logic as provided above. Even though in the multi-cell scenario further aspects play role, including the effects of RIS configuration on cell loads and the consequent effects of inter-cell interference, the bottom-line impact of the RIS location is still marginal. Lastly, note that the throughput performance is substantially worse in the multi-cell scenario, which is simply due to the presence of inter-cell interference.

V. Conclusions

We developed and evaluated radio resource management algorithms for RIS-enabled mobile networks. Our scenario-based analyses demonstrated that substantial performance gains are attainable from optimised RIS utilisation. The proposed algorithms significantly improve the 10^{th} user throughput percentile, achieving 48% and a 100% gains in single- and multi-cell scenarios, respectively. Furthermore, proposed *Algorithm 2* was shown to enhance network coverage in single-cell scenarios, while no coverage gains were observed in the multi-cell scenarios. We further observed that the specific deployment location of a RIS does not significantly affect the bottom-line performance gains, noting that distinct user groups experience different degrees of benefits under different RIS deployment locations. Future work will explore AI-based enhancements and assess the impact of realistic channel state acquisition techniques on RIS integration in 6G networks. To strengthen evaluation, future work should further combine simulations with real-world testing via field trials or testbeds.

Acknowledgment

This research was supported by the National Growth Fund through the Dutch 6G flagship project “Future Network Services”.

References

[1] C. Huang, A. Zappone, G. C. Alexandropoulos, M. Debbah and C. Yuen, ‘Reconfigurable intelligent surfaces for energy efficiency in wireless communication,’ *Transactions on Wireless Communications*, vol. 18, no. 8, Aug. 2019.

[2] Q. Wu and R. Zhang, ‘Intelligent reflecting surface enhanced wireless network via joint active and passive beamforming,’ *Transactions on Wireless Communications*, vol. 18, no. 11, Nov. 2019.

[3] X. Yu, D. Xu and R. Schober, ‘MISO wireless communication systems via intelligent reflecting surfaces’, *Proceedings of ICCC ‘19*, Changchun, China, 2019.

[4] C. Huang, R. Mo and C. Yuen, ‘Reconfigurable intelligent surface assisted multiuser MISO systems exploiting deep reinforcement learning,’ *Journal on Selected Areas in Communications*, vol. 38, no. 8, 2020.

[5] C. Huang, G. C. Alexandropoulos, C. Yuen and M. Debbah, ‘Indoor signal focusing with deep learning designed reconfigurable intelligent surfaces’, *Proceedings of SPAWC ‘19*, Cannes, France, 2019.

[6] Z. Zhang, T. Jiang, and W. Yu, ‘User scheduling using graph neural networks for reconfigurable intelligent surface assisted multiuser downlink communications,’ *Proceedings of ICASSP ‘22*, Singapore, 2022.

[7] Y. Zhu, M. Li, Y. Liu, Q. Liu, Z. Chang, and Y. Hu, ‘DRL-based joint beamforming and BS-RIS-UE association design for RIS-assisted mmWave networks’, *Proceedings of WCNC ‘22*, Austin, USA, 2022.

[8] 3GPP, *‘Study on channel model for frequencies from 0.5 to 100 GHz’*, TR138.901, v16.1.0, 2019.

[9] F. Gunnarsson *et al.*, ‘Downtilted base station antennas - A simulation model proposal and impact on HSPA and LTE performance’, *Proceedings of VTC ‘08*, Calgary, Canada, 2008.

[10] T.-H. Vu and S. Kim, ‘Performance analysis of full-duplex two-way RIS-based systems with imperfect CSI and discrete phase-shift design’, *Communications Letters*, vol. 27, no. 2, 2023.

[11] W. Tang *et al.*, ‘Wireless communications with reconfigurable intelligent surface: path loss modeling and experimental measurement’, *Transactions on Wireless Communications*, vol. 20, no. 1, 2021.

[12] H. Friis, ‘A note on a simple transmission formula’, *Proceedings of the IRE*, vol. 34, no. 5, 1946.

[13] R. Fraile, J. F. Monserrat, J. Gozalvez and N. Cardona, ‘Mobile radio bi-dimensional large-scale fading modelling with site-to-site cross-correlation’, *Eur. Trans. on Telecommunications*, vol. 19, no. 1, 2008.

[14] Z. Lai, N. Bessis, G. de la Roche, P. Kuonen, J. Zhang and G. Clapworthy, ‘The characterisation of human body influence on indoor 3.5 GHz path loss measurement’, *Proceedings of the WCNC ‘10 workshops*, Sydney, Australia, 2010.

[15] Fraunhofer, *‘Quadriga – The next generation radio channel model’*, www.quadriga-channel-model.de, 2020.

[16] T. Yoo and A. Goldsmith, ‘On the optimality of multiantenna broadcast scheduling using zero-forcing beamforming’, *Journal on Selected Areas in Communications*, vol. 24, no. 3, 2006.

[17] P. Bender, P. Black, M. Grob, R. Padovani, N. Sindhushyana and A. Viterbi, ‘CDMA/HDR: a bandwidth efficient high speed wireless data service for nomadic users’, *Commun. Mag.*, vol. 38, no. 7, 2000.

[18] S. Agarwal, *‘Development and assessment of resource management solutions for throughput enhancement in a RIS-aided mobile network’*, MSc thesis, Delft University of Technology, 2023.